P. Belo, V. Parail, G. Corrigan, D. Heading, W. Houlberg, P. Monier-Garbet,
J. Ongena and JET EFDA contributors

Impurity Penetration through the Edge Transport Barrier

Impurity Penetration through the Edge Transport Barrier

P. Belo[1], V. Parail[2], G. Corrigan[2], D. Heading[2], W. Houlberg[3], P. Monier-Garbet[4],
J. Ongena[5], and JET EFDA contributors*

[1]*EURATOM/IST Fusion Association, Centro de Fusão Nuclear, Av. Rovisco Pais 1049-001 Lisboa Portugal*
[2]*EURATOM/UKAEA Fusion Association, Culham Science Centre, Abingdon OX14 3DB, UK;*
[3]*Oak Ridge National Laboratory, Oak Ridge, TN 37831*
[4]*Association Euratom-CEA, Cadarache 13108 SAINT PAUL LEZ DURANCE, FRANCE*
[5]*Laboratoire de Physique des Plasmas-Laboratorium voor Plasmafysica, Association EURATOM-Belgian
State, Ecole Royale Militaire-B-1000 Brussels, Koninklijke Militaire School[b], Belgium*
[a]*Researcher at FWO Vlaanderen*
[b]*Partner in the trilateral Euregio Cluester (TEC)*
* See annex of J. Pamela et al, "Overview of Recent JET Results and Future Perspectives",
Fusion Energy 2000 (Proc. 18th Int. Conf. Sorrento, 2000), IAEA, Vienna (2001).*

ABSTRACT.

The ELMs in H Mode plasmas manifest themselves as short bursts of increased edge transport, which expel energy and particles, including impurities from the plasma edge to the SOL and further towards target plates and limiters [1, 2]. On the other hand, ELMs are considered beneficial events with respect to impurities since they can prevent impurities from accumulating in the plasma core. JET has recently performed an experiment in which controlled influx of noble gas impurities was successfully used in order to reduce the amplitude and frequency of type-I ELMs. An interesting correlation between the level of the main gas puffing and the radial redistribution of impurities has been found in this experiment. Namely, it was shown that impurities are contained near the separatrix in discharges with a relatively strong level of main gas puffing. Reduction of the puffing below a certain level leads to impurity accumulation in the core followed by thermal collapse. The present paper describes the results of predictive modelling of impurity seeding experiments on JET using a coupling of the 1.5D core transport code JETTO (for the main ions) and 1D transport code SANCO (for impurities). Two sets of boundary conditions for the density and temperatures, which correspond to two different deuterium gas puffing rates, were used in the modelling. An explanation of experimentally observed phenomena is presented.

1. INTRODUCTION

The danger posed by periodic particle and energy bursts coming from the edge of the plasma during a Type I ELM towards plasma facing components was realised years ago [1] and studied in many tokamaks including JET [2]. The increased power loads are not so harmful for present day tokamaks but they present one of the greatest challenges for future tokamak like ITER [3]. Several techniques for ELM mitigation have been proposed and studied on many tokamaks, including ELM mitigation by controlled impurity puffing [4-9]. Impurities like Argon and Neon that have high recycling rates can create poloidally and toroidally uniform mantle near the separatrix in order to increase evenly the radiation and reduce the power flux through the separatrix both during and between ELMs, using the diffusivity model. This should reduce the power load on a divertor target plate as well as reduce ELM amplitude and frequency.

It was also found that controlled impurity puffing can result in an increase of confinement time and stored energy in some other tokamaks like TEXTOR [5], DIII-D [6], AUG [7] and JT-60U [8] due to a partial suppression of plasma turbulence, particularly Ion Temperature Gradient (ITG) mode [9].

The radiating mantle experiments at JET were done in two different magnetic configurations: low and high upper triangularities [10, 11]. In low triangularity plasmas, impurity and deuterium puffing cause temporary degradation of plasma confinement followed by a transition from Type I to Type III ELMs [11, 12]. The energy and particle confinement recover after the end of strong puffing so that the plasma re-establishes the type I ELMs [11]. With high triangularity, JET plasma manage to stay in type-I ELMy H-mode even during a continuous deuterium gas puffing and 'blips' of impurity

puffing without noticeable degradation in plasma confinement with the reduced ELM frequency and amplitude [10, 11]. On the other hand these experiments have shown that the level of gas puffing should be kept above a certain level, below which impurities start to accumulate in the core and eventually cause a radiative collapse.

The main goal of this paper is to identify the main theoretical mechanisms of impurity accumulation in ELMy H-mode by comparing predictive modelling of a series of ELMy H-mode JET plasmas with experiment.

The paper is organised as follows. Section II describes the main experimental observations from JET. The transport mechanisms responsible for impurity redistribution in the ELMy H-mode are discussed in section III. Section IV is devoted to the modelling results, which is followed by a summary and conclusions in section V.

2. EXPERIMENTAL OBSERVATIONS.

It has been discussed already in many publications [3, 11, 13, 14] that impurity accumulation in the central part of the plasma column usually happens after the disappearance of sawteeth. The reason for this is that sawteeth prevent impurity accumulation by flattening all core plasma profiles, including the impurity density. After the disappearance of sawteeth the main ion density tends to peak in discharges with NBI heating due to a combined action of an NBI-based central particle source, inward velocities of the anomalous transport for low density plasmas and to the Ware pinch velocity of the neoclassical transport for high density plasmas [15, 16]. If neo-classical transport is the main contributor to particle transport, impurity accumulation is expected when density peakedness (which can be characterised by the inverse density gradient scale length) $L_n^{-1} \equiv \frac{|\nabla n_i|}{n_i}$) exceeds the corresponding critical ion temperature gradient inverse scale length $L_n^{-1} \equiv \frac{|\nabla n_i|}{n_i}$: $L_n^{-1} \geq \frac{H}{K^{\nu} L_{T_i}}$, where K depends on ion collisionality [17]. Experiments confirmed this trend [11, 13, 18]. Moreover it was shown that sawtooth suppression in JET as well as central impurity accumulation could be avoided by applying a few MW of ICRH power with centrally peaked power deposition. The later leads to a peaking of the temperature profile and to a flattening of the density profile. It is worth noting here that there is an alternative explanation to the latter trend based on the fact that central heating should increase the level of ITG turbulence, which stops the neoclassical terms from being the major contributor to particle transport for the main ions [15].

In this paper we will discuss a broader issue of impurity accumulation that includes the plasma edge as well as the core. Figure 1 shows the main time traces for a pair of JET shots from the 2001 campaign: Pulse No: 53145 and Pulse No: 53146. The discharges have the same current, toroidal field, magnetic configuration and heating power. They also have the same rate of argon impurity seeding. The only difference was in the main gas puffing scheme: Pulse No: 53146 had a reduced level of deuterium puffing starting from t = 22s. This reduction of the gas puffing rate results in a sudden increase of the radiation, which indicates an increase of impurity particle content in the core

2

and eventually leads to a collapse of the plasma energy content. This experimental observation is actually quite reproducible. Figure 2 shows a similar pattern of behaviour for the discharge with Ar seeding and a monotonically decreasing level of the main gas puffing. One can observe that the radiated power starts to grow rapidly once the main gas puffing rate drops below some critical level (which is in fact very similar to the critical rate for the Pulse No:53245 from Figure 1). It can be seen from Fig.2 that the application of Ar seeding (which starts at t = 20s) leads to an increase in the level of radiated power (b), which is immediately followed by the reduction in ELM frequency. Note that for the first 2-3 seconds of Ar seeding there is no detrimental effect of the radiation on the energy content (a). Degradation in plasma confinement comes later, at t ≥ 22s, when the radiated power starts to rise in time exponentially and exceeds the level of plasma heating by NBI.

Figure 3 shows reconstructed radiated power density profiles for Pulse No's:53549 and 53550 at three times: t = 20.5s (half a second after the beginning of Ar seeding in Pulse No: 53550); t = 21.5s (half a second before the onset of the exponential rise in the radiated power in Pulse No: 53550) and at t = 22.5s (half a second after the onset). It is clearly seen that the radiated power profiles at t < 22s are similar for the two pulses with the main difference coming from the level of the radiated power but not in its radial distribution. Only for t ≥ 22s is there a significant change in the core radiated power for the Pulse No: 53550. This time coincides with the time when the main level of gas puffing decreases below the critical level, found for the Pulse No:53146 from Figure 1. In other words, it looks like strong gas puffing manages to keep impurities mainly outside the separatrix or very close to it (within the Edge Transport Barrier (ETB)). On the other hand, reducing the level of the main gas puffing opens the way for impurities to enter the plasma core in an uncontrollable way, which ends up in the thermal collapse. Since "controllable" impurity radiation is considered as a viable option to reduce the amplitude and the frequency of type-I ELMs in tokamak-reactor, it is very important to understand which physics processes control the redistribution of impurities inside separatrix.

3. IMPURITY TRANSPORT

Both anomalous and neoclassical transport models contribute to impurity transport in the plasma core. We will use an empirical Bohm/gyroBohm model [19] for anomalous transport. Theory predicts that impurities reduce the level of anomalous transport, at least the part of it that is related to ITG instability [9], and we will take this effect into account in our modelling. Neoclassical transport plays an important role in those areas of plasma where anomalous transport is fully suppressed or at least weakened [15, 18]. ELMy H-mode has two regions of reduced anomalous transport: a very central part of plasma and the edge transport barrier. We are most interested in studying the ETB region because this is the region that the impurity must cross before penetrating deeper into the plasma volume. We assume in our analysis that the ETB is a narrow region (with the width $\Delta \approx 3$cm for JET) in which anomalous transport is fully suppressed between ELMs. We will use a simple model for ELMs, which is based on ideal ballooning instability. The model has been tested on a

3

number of JET shots [20, 21] and it is implemented in JETTO in the following way. The code checks the normalised pressure gradient $\alpha \equiv \frac{-2\mu_0 R q^2}{B_\phi^2} \cdot \frac{\partial p}{\partial r}$ within the ETB and compares it with the critical parameter α_{crit}, which destabilises the ballooning mode. The code increases all anomalous transport coefficients within the ETB for a short period of time Δt (with $\Delta t \leq 0.3$msec) to simulate an ELM. The ELM amplitude is a free parameter, which is adjusted so that the energy drop during the ELM is close to the experimentally observed range $\Delta W/W \approx (2 \div 5)\%$.

A full matrix of the neoclassical transport coefficients for impurities and the main ions is taken from NCLASS [22]. For this paper, the neo-classical convective particle velocity is probably the most important part of this matrix, since it is believed to be responsible for impurity accumulation in the plasma core. Generally the neoclassical flux not including the Ware pinch can be written in the following form [22]:

$$\Gamma_i^{neo} = -Z\Gamma_z^{neo} = -\frac{n_i D}{2}\left[K\left(\frac{1}{n_i}\frac{dn_i}{dr} - \frac{1}{Zn_z}\frac{dn_Z}{dr}\right) + \frac{H}{T_i}\frac{dT_i}{dr}\right] \tag{1}$$

where n_z and n_i are the densities of impurity and the main ions respectively, Z is the charge of the impurity, $D \propto n_z$ is the neoclassical diffusion coefficient and K and H are functions of dimensionless plasma parameters, including ion collisionality (see [17]). Theory predicts that coefficient $K > 0$ so that the first term in the right hand side of (1) causes an inward convective velocity for impurities if $\frac{dn_i}{dr} \dagger 0$ for the whole range of collisionalities. The coefficient H on the other hand changes sign depending on the collisionality of both main and impurity ions. Ar is normally in the Pfirsh-Shlüter regime in JET ELMy H-mode plasma, but experiments under consideration only used traces of Ar. From the neoclassical approximation [22, 24] the main ions are the major contributors for the viscosity in this case, and they are mainly in the banana regime, where $\frac{H}{K} \approx -0.5$ so that the third term in the right hand side of (1) evokes an outward convective velocity or "screening effect", if $\frac{dT_i}{dr} \dagger 0$. The competition between these two terms determines the fate of impurities: they can be stopped at the edge in the case of a relatively strong temperature gradient (if $\frac{1}{n_i}\left|\frac{dn_i}{dr}\right| \dagger \frac{|H|}{T_i}\left|\frac{dT_i}{dr}\right|$) or they can penetrate deep into the plasma core in the opposite case of a weak temperature gradient. Actually the main aim of our numerical simulation will be to prove this statement and to evaluate conditions when the situation changes from holding impurities at the edge to allowing them to accumulate in the core.

4. PREDICTIVE MODELLING

We use the 1.5 D transport code JETTO for numerical simulations. We start our modelling by trying to reproduce plasma parameters in the reference Pulse No: 53549 without Ar puffing. It was therefore assumed that the level of Z_{eff} is fixed and the main impurity is carbon. It is worth noting here that modelling of the plasma with a strong external source of cold neutrals (gas puffing) is a

4

notoriously difficult task. The problem is that there is no reliable model for the neutrals that recycle from the complex geometry of the wall and target plates. Even 2D SOL codes (like EDGE2D/NIMBUS and B2/EIRENA) have problems with recycled neutrals (although they treat penetration of neutrals through the SOL much better that 1.5D core transport codes). Therefore we decide to use our usual prescription about the main ion density evolution in the absence of divertor pumping: we assume that wall recycles 100% of ions so that R=1 (all outgoing ion flux is returned back as cold neutrals). We select additional gas influx on the level that brings the average ion density in agreement with experiment. Our experience with a combined core-SOL transport code COCONUT [25] shows that external gas puffing influences the ion density and temperature near the separatrix (which are used as boundary conditions in JETTO). To take this effect into account we can increase the edge density in accord with the level of gas puffing and we can simultaneously decrease the edge temperature as gas puffing rises.

Figures 4 and 5 show some characteristic time traces and plasma profiles (simulated and taken from experiment) for the Pulse No: 53549. We can conclude that modelling manages to reproduce quite well all main plasma profiles as well as plasma dynamics (in terms of ELM frequency and amplitude).

Predictive modelling of impurity evolution is the next logical step to take. We employ a recently developed link between JETTO (which simulates evolution of the main ion density together with the electron and ion temperature and current profiles) with the 1D code SANCO. SANCO solves continuity equations for all ionisation stages of one or two impurity species. It takes into account all ionisation, recombination and radiation processes as well as the full matrix of neoclassical transport coefficients and that of anomalous transport, which all come from JETTO. There is one significant difference between JETTO and SANCO in terms of how they impose boundary conditions. While JETTO imposes boundary conditions at the separatrix, SANCO extends its computational grid into the SOL. Since SANCO is a 1D code it simulates longitudinal transport in the SOL by introducing finite confinement time along the field lines to the divertor in the SOL in addition to losses due to perpendicular transport. We assume in this paper that all impurities come from the puffing of either Ar or Ne, which both have a 100% wall recycling. It is assumed in all the simulations that both anomalous and neoclassical perpendicular transport coefficients are extended into the SOL, although it is clear that this assumption can be used as an example only.

Two sets of boundary conditions were used in predictive modelling to prove the importance of the gas puffing in an attempt to avoid impurity accumulation in the core, shown in Fig.6. We keep plasma parameters at the separatrix constant in the first case [with T_e ($\rho = 1$) = T_i ($\rho = 1$) = 10^2 eV and n_i ($\rho = 1$) = $5 \cdot 10^{19}$ m^{-3}, which corresponds to a constant, high level of gas puffing. We then reduce edge density and increase edge temperature in the second run (with T_e ($\rho = 1$) = T_i ($\rho = 1$) increasing in time from 100eV to 400eV and ion density decreasing from n_i ($\rho = 1$) = $5 \cdot 10^{19}$ m^{-3} to n_i ($\rho = 1$) = $2 \cdot 10^{19}$ m^{-3} at the end of run) to simulate the decrease of the gas puff [25]. It is worth noting here that we apply a sawtooth reconnection model in both runs. Each sawtooth crash

redistributes evenly the electron and ion temperatures as well as the main ion density and all impurities across the reconnection area (up to $\rho \leq 0.7$ in our case). To simulate the experimentally observed disappearance of sawteeth in a later phase of the Pulse No: 53550 (with impurity injection) we turn off the sawtooth reconnection model at $t = 23s$ in both runs with impurity injection. Figure 7 shows the main time traces for two simulations. The same level of impurity (Ar in our case) puffing was used in both runs. One can observe very similar initial evolution of all main plasma parameters (due to the similarity in the boundary conditions at initial stage of the simulations). Starting from $t = 21.5$ s, however, the edge density goes down and the edge temperature goes up in "red" case. This gradual change in the boundary conditions causes a dramatic transformation in impurity behaviour: they start to penetrate through the edge transport barrier and accumulate in the core. The reason for such transformation is the convective velocity for impurities, which changes sign from positive to negative within the edge barrier. Figure 8 shows the radial distribution of the convective velocity, averaged over all ionisation stages, and the impurity density for two time slices: $t = 21s$ and $t = 23s$ for Pulse No: 53550. At 21.0 s the two runs have the same boundary conditions and both have the same positive convective velocity, leading to a accumulation of impurities outside separatrix, in the SOL. At $t = 23s$ after the step down in the edge density and step up in the edge temperature in the "red" case, the convective velocity for Pulse No: 53550 has a different, negative sign. This allows impurities to penetrate through the ETB and to accumulate deeper in the core, changing both the level and the pattern of the radiated power. Simulations show that higher level of core radiation effectively reduces the heat flux across the separatrix, which results in a decrease of ELMs frequency [26].

For these two runs the ELMs make different contributions to the impurity transport. Each ELM drives the impurity toward the centre in the "black" case of strong gas puffing, as it is shown in Figure 9. However, the impurity content both in the SOL and in the core recovers its pre-ELM level in 50ms after the end of ELM. Keeping in mind that experimentally observed ELM repetition rate is very low, $\Delta t_{ELM} = 210ms$, we conclude that transport between ELMs is more important for impurity redistribution than transport during the ELM in type-I ELMy H-mode JET plasmas. It is worth noting here that ELMs are usually considered as beneficial factor, which keeps impurities away from the core. The modelling shows, however, that if ELMs have a diffusive nature, they can actually drive impurities toward the plasma core as well.

Figure 10 shows the time evolution of impurity content in the "red" case of low gas puffing, where the pinch velocity turns negative for impurities. One can observe that each ELM expels impurities from the core to the SOL, in accordance with expectations. However, the impurity density recovers its pre ELM shape in 30 ms after the ELM owing to an inward neoclassical convective velocity. Note that we assume in the above-mentioned simulations that impurities like Ne or Ar can not be removed from the SOL by pumping. In real experiments gaseous impurities can be removed from the SOL by the cryogenic pump. To take this effect into account we reduce the wall recycling to $R = 0.8$ in further simulations. Specifically, we study how ELM frequency influences the impurity content in the plasma with the cryogenic pump. To do this we used different values of the critical

6

pressure gradient for the ballooning stability, which allows us to keep the values of the inward convective velocity the same for all cases. The result of the modelling is shown in Figure 11 and allows us to conclude that the out flux rate of impurities is proportional to the ELM frequency, as it was observed in experiment.

Finally, we study how a sawtooth crash influences the radial distribution of impurity particles and the radiated power. Figure 12 shows the result of the modelling for the case when the impurity particles penetrate the ETB but do not accumulate in the core due to a small outward neoclassical convective velocity. The sawtooth crash, observed in figure 12, redistributes the impurities uniformly over the reconnection region of the plasma. This redistribution of the impurity over the plasma core leads to an increase in the level of the radiated power from the plasma core in this particular case. If the impurity distribution were peaked in the plasma centre the effect of the sawtooth crash would be opposite. It is important to stress here that the thermal collapse of plasma energy content observed in our simulation happens not because of the disappearance of the sawteeth but because of the acquired ability of impurities to penetrate inside the ETB. The latter process is controlled by the neoclassical convective velocity within ETB, which depends on the fine details of the ion temperature and density profiles within the edge barrier.

SUMMARY AND CONCLUSIONS
In this paper we simulate the effects on the impurities of the deuterium gas puff and the ELMs using the JETTO and SANCO codes. Although the Ar is in the Pfirsch-Schlüter regime and the main ions are in the banana regime, the neoclassical impurity transport is in the banana regime. The result from the simulations explains the increase of the radiation after the reduction of the gas puff. Reducing the gas puff increases the main ion gradient at the ETB and decreases the ion temperature gradient, changing the convective velocity sign from positive to negative (from outward to inward). This permits the impurities to penetrate the ETB and accumulate between $0.6 < \rho \leq 0.95$. In the later time can lead into a radiactive collapse.

The ELM contribution to preventing impurity accumulation is not so important as either the deuterium gas puff or the outward convective velocity due to high ion temperature gradient and low main ion density gradient. Nevertheless, higher ELM frequency reduces the number of impurity particles going to the core when the impurity recycling $R < 1.0$, to simulate the cryogenic pump.

It was also shown that the sawtooth crash does not have any effect on the impurities when the convective velocity is outward in the ETB. But it contributes to a fast impurity accumulation when the convective velocity is inwards. This accumulation is due to the fact that the impurity distribution is still hollow for $\rho \leq 0.6$. But we can conclude that a sawtooth crash prevents impurity accumulation for peaked impurity profiles.

and IST, was performed under the European Fusion Development Agreement. The views and opinions expressed herein do not necessarily reflect those of the European Commission and IST.

REFERENCES

[1]. Zohm,H., Plasma Phys. Control. Fusion, **38** (1996), 1213

[2]. Loarte, A., et al, Plasma Phys. Control. Fusion, **45** (2003), 1549

[3]. Frederici, G., et al, Plasma Phys. Control. Fusion, **45** (2003), 1549

[4]. Ongena, J., et al, Plasma Phys. Control. Fusion, **43** (2001), A11

[5]. Ongena, J., et al, Plasma Phys. Control. Fusion, **41** (1999), A379

[6]. McKee, G., Burrell, K., Fonck, R., Jackson, G., Murakami, M., Staebler, G., Thomas, D., and West, P., Physical Review Letters, **84** (2000), 1922

[7]. Kallenbach, A., et al, Plasma Phys. Control. Fusion, **38** (1996), 2097

[8]. Kubo, H., et al, Physics of Plasmas, **9** (2002), 2127

[9]. Tokar, M.Z., Plasma Phys. Control. Fusion, **38** (1999), L9

[10]. Puiatti, M.E. et al, Plasma Phys. Control. Fusion, **44** (2002), 1863

[11]. Maddison, G.P., et al, Plasma Phys. Control. Fusion, **45** (2003), 1657

[12]. Strachan, J-D, et al, Plasma Phys. Control. Fusion, **42** (2000), A81

[13]. Nave F., et al, Nuclear Fusion, **43** (2003), 1204

[14]. Puiatti, M.E., et al, Simulation of the time behaviour in JET Ar-seeded discharges and its relation with sawtooth, to be published

[15]. Stober, J., et al, Nuclear Fusion, **43** (2003), 1265

[16]. Angioni, C., et al, phys. of Plasmas, **10** (2003) 3225

[17]. Hirshman, S.P., Sigmar, D.J., Nuclear Fusion, **21** (1981), 1079

[18]. Wade, M.R., Houlberg, W.A., and Baylor, L.R., Physical Review Letters, **84**, (2000) 282

[19]. Cherubini, A., Erba, M., Parail,V., Epringmann, E. and Taroni, A. Plasma Phys. Control. Fusion, **38** (1996), 1421

[20]. Erba, M., Cherubini, A., Parail,V., Plasma Phys. Control. Fusion, **39** (1997), 261

[21]. Parail, V., Plasma Phys. Control. Fusion, **44** (2002), A63

[22]. Houlberg, W.A., Shaing, K.C., Hirshman, S.P., Zarnstorff, M.C., Phys. of Plasma, **4** (1997), 3230

[23]. Wenzel, K.W., Sigmar, D.J., Nuclear Fusion, **30** (1990), 1117

[24]. Rutherford, P.H., Hirshman, S.P., Jensen, R., Post, D.E. and Seidl. F.G.P., Impurity Transport in Tokamaks, International Symposium on Plasma Wall Interaction, Jülich, Germany, 18-22 October 1976.

[25]. Lönnroth S-J, et al, Plasma Phys. Control. Fusion, **45** (2003), 1689

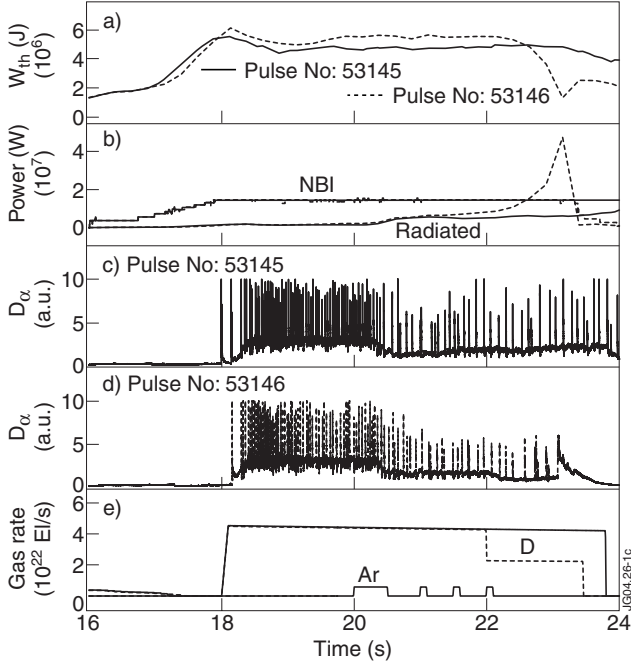[26]. Monier-Garbet, P. et al, private communication, IAE workshop on ELMs, 24-26 June 2002

Figure 1: Energy content (a), heating power and radiated power (b), Dα signal (c-d) and gas puffing rate(e) for Pulse No: 53145 (full line) and Pulse No: 53146 (dashed line).
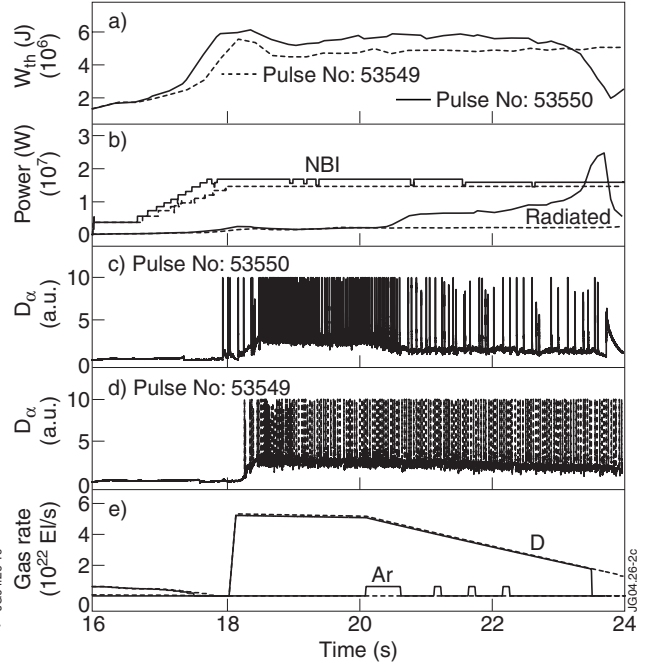

Figure 2: same parameters as on Figure 1 for the Ar seeded Pulse No: 53550 (full line) and reference Pulse No: 53549 without Ar (dashed line)
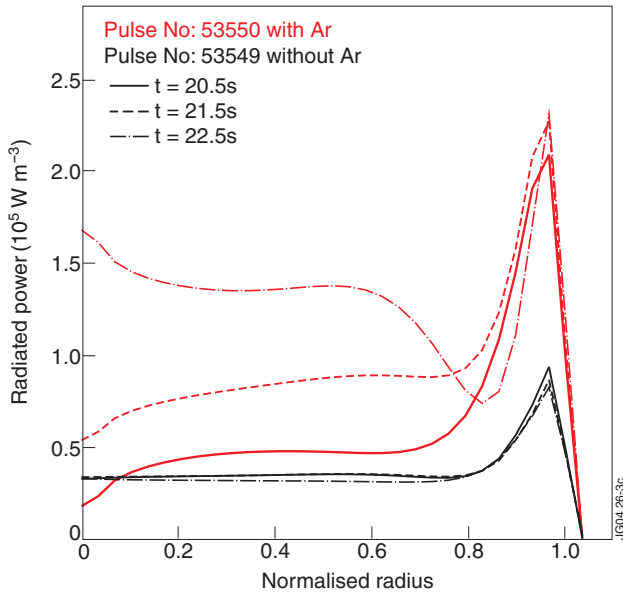

Figure 3: Measured radiated power profile for a pair of shots from Figure 2 (Pulse No: 53550 with Ar, red and Pulse No: 53549 without Ar, black) for three time slices: t = 20.5s, t = 21.5s and t = 22.5s.
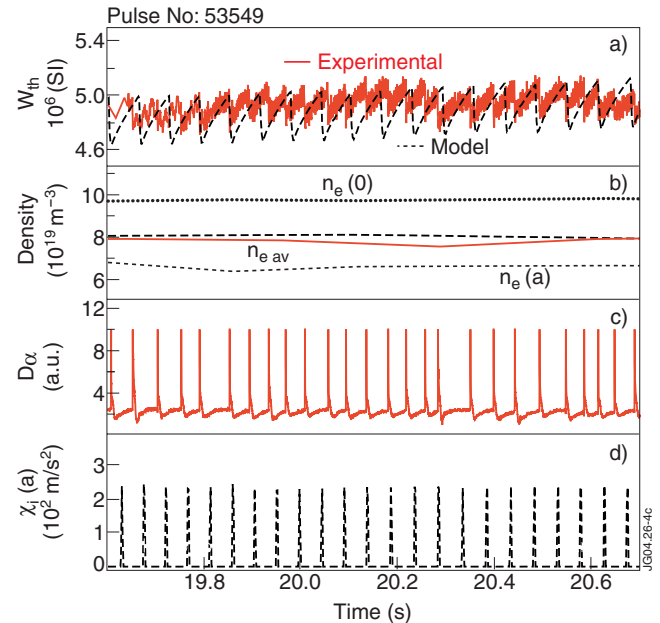
Figure 4: Experimental and simulated time traces for the reference Pulse No: 53549 without Ar puffing.
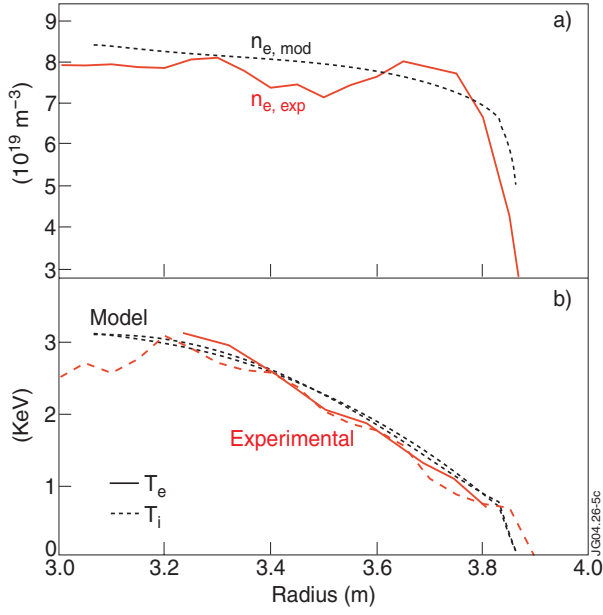
Figure 5: Experimental and simulated profiles for the reference Pulse No: 53549 without Ar puffing
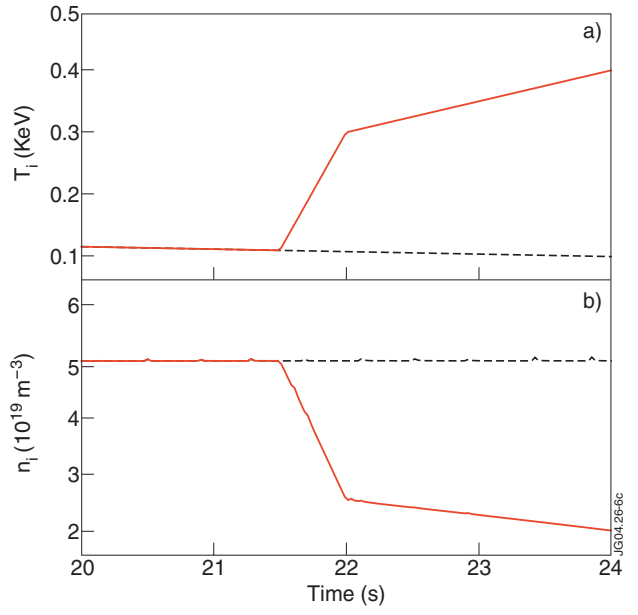
Figure 6: Time evolutions of the ion temperature (a) and ion density (b) boundaries for simulation with impurity
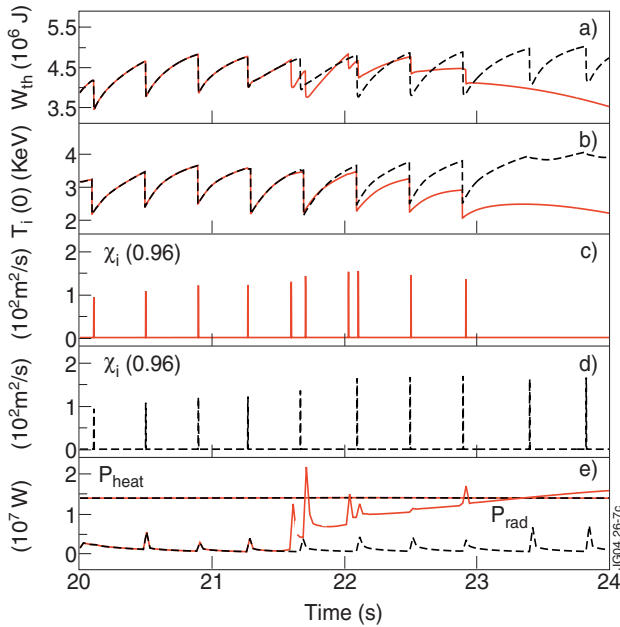
Figure 7: Time traces for the run with the same rate of impurity puff but different boundary conditions: constant temperatures and density (black) and rising temperature and falling density (red).
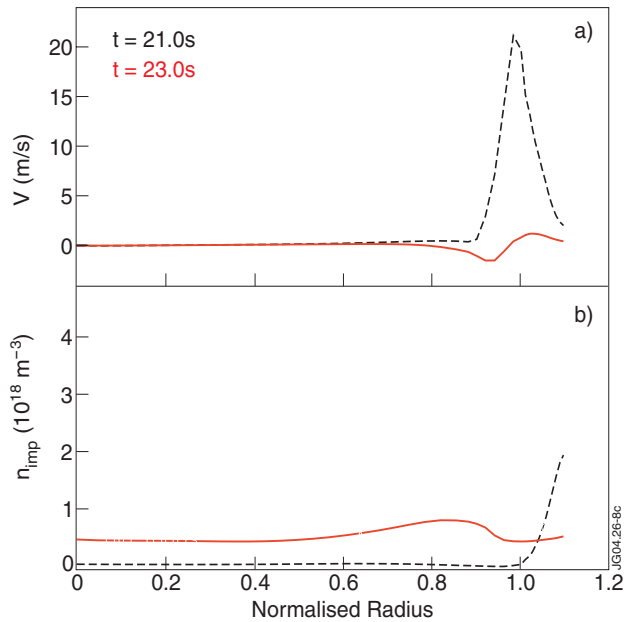

Figure 8: Radial distribution of convective velocity density of impurity before (black) and after (red) transition to a lower level of gas puffing.
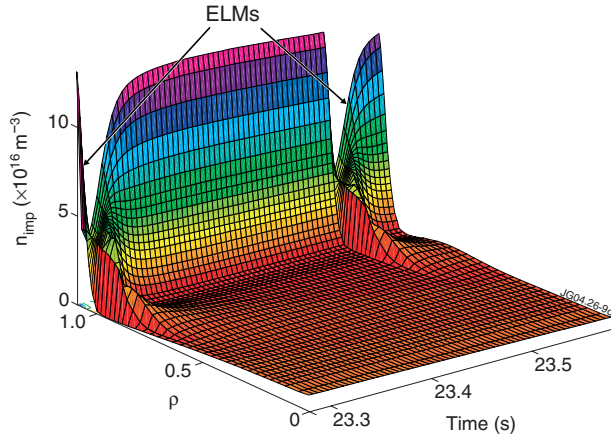
Figure 9: Evolution in time of the impurity density profiles between two ELMs for the "black" case.
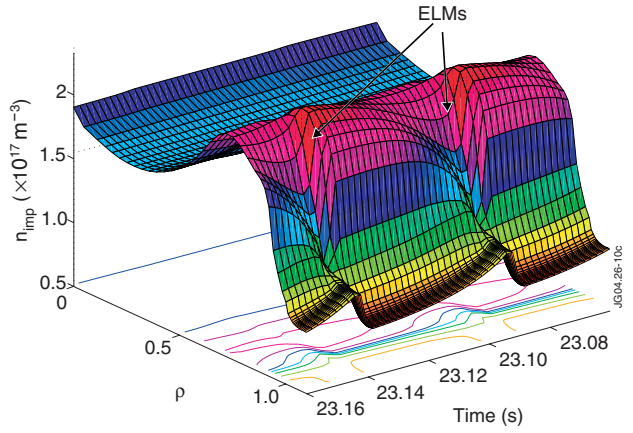

Figure 10: Evolution in time of the impurity density profiles between two ELMs for the "red" case.
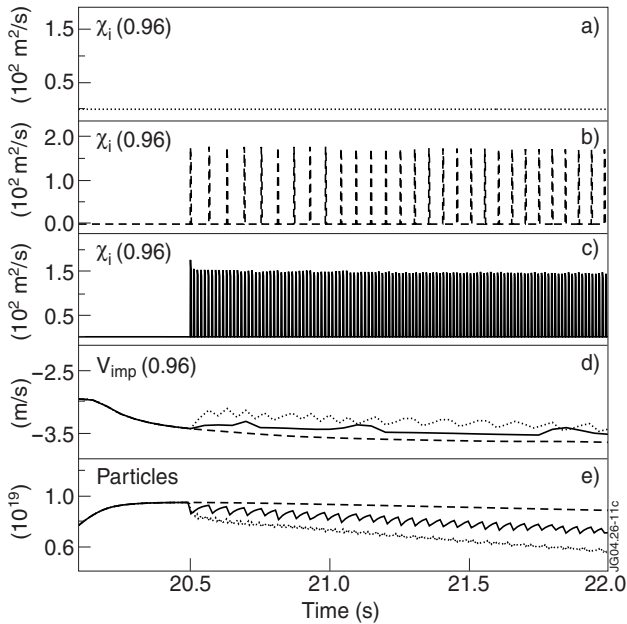

Figure 11: Time traces at the ETB for different ELM frequencies after 20.1 sec: no ELMs blue; ELM frequency of 20Hz red and ELM frequency of 70Hz yellow; of the thermal ion transport, average velocity over the all ionization stages and the total number of impurity particles inside the separatrix.
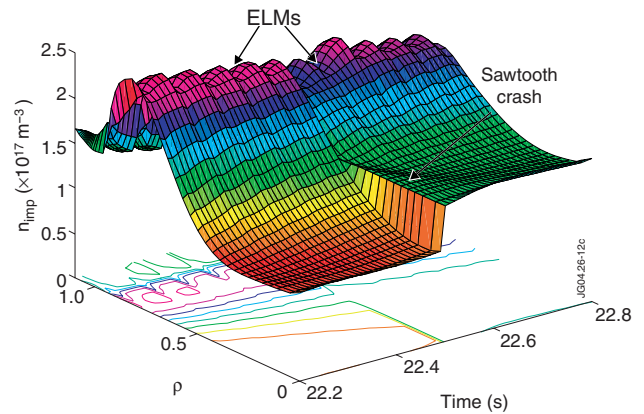

Figure 12: Evolution in time of the impurity density profiles during ELMs and a sawtooth crash for the "red" case".

11